THE OHIO STATE UNIVERSITY

A SENIOR HONORS THESIS

Optical Detection of Acoustically Driven Ferromagnetic Resonance

---

Author:
Qiaochu GUO

Supervisor:
Dr. P. Chris HAMMEL
Dr. Jinwoo HWANG

Presented in Partial Fulfillment of the Requirements for
Graduation *with research distinction in Engineering Physics*
in the undergraduate colleges of The Ohio State University

April 14, 2017

Abstract

Optical Detection of Acoustically Driven Ferromagnetic Resonance

by Qiaochu GUO

The nitrogen-vacancy (NV) center is a diamond defect that has been considered a potential material to develop nanoscale magnetometers. In this study, we use NV-centers in diamond to optically detect ferromagnetic resonance (FMR) driven by surface acoustic waves. An experimental setup was designed to simultaneously measure the fluorescence of NV-diamonds and electrical transmission signal when the ferromagnetic sample reaches FMR. We investigated the correlation between NV-center fluorescence and input microwave frequency, external magnetic field, and position relative to the ferromagnetic material. Moreover, we developed a scanning magnetometer by attaching NV-diamonds to the tip of an AFM probe. An optically detected magnetic resonance (ODMR) spectrum is obtained from the NV-diamond probe. The NV-diamond probe will be used in future studies to understand the spatial dependence of the coupling between NV-centers and ferromagnetic materials.

Contents

List of Figures

List of Tables

Chapter 1

Optical Detection of Acoustically Driven Ferromagnetic Resonance

1.1 Introduction

With the development of magneto-electronics and spin-based device technologies, studies of ferromagnetic resonance (FMR) at the micro-and nano- scale have become an area of major research focus. An emerging method for optically detecting magnetic resonance uses nitrogen-vacancy (NV) centers in diamond. Detection of magnetic dynamics and resonance at the nanoscale with extreme sensitivity can be achieved due to the spin-dependent fluorescence of NV-centers [1] [2] [3]. Our group has recently made the first demonstration of FMR detection using NV-based Optically Detected Magnetic Resonance (ODMR)[4] [5]. Our collaborators have recently demonstrated a novel technique of acoustically driven FMR (ADFMR) through magnetostriction–for magnetostrictive ferromagnetic materials, elastic deformations will result in change of magnetization and vice versa [6]. Since acoustic waves travel at the speed of sound, they have much shorter wavelengths compared to microwaves, thus allow us to design magnetic devices of size several orders of magnitude smaller than devices with traditional electromagnetic excitation [7]. Moreover, driven by electric field instead of current, ADFMR avoids power dissipation due to electron

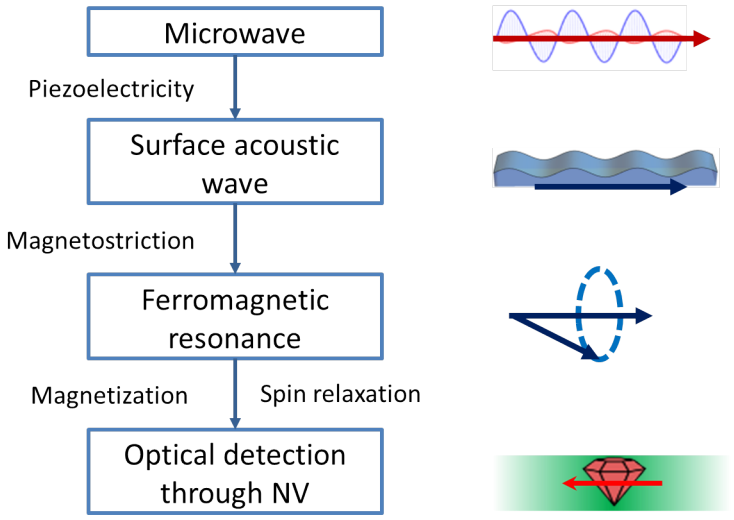

FIGURE 1.1: The basic mechanism of the optically detected ADFMR system

flow and can be applied in low-power devices [6]. Here, we use surface acoustic waves (SAWs) in an underlying piezoelectric substrate to generate elastic deformations in a ferromagnetic thin film and thereby excite FMR. Detecting ADFMR with NV-centers not only provides us a means to study ADFMR on smaller length scales, but also allows us to investigate of the coupling between NV-centers and ferromagnetic materials. In this experiment, we developed a platform to study investigate the interactions between NV-centers, surface acoustic waves and ferromagnetic materials. The basic mechanics of the system is shown in Figure 1.1.

1.2 Background

1.2.1 Nitrogen-vacancy Centers in Diamond

Diamond consists of five carbon atoms in each of its unit cell. Ideal homogeneous diamonds are transparent and colorless. The impurities and defects in diamond are very stable and have

various interesting physical and chemical properties [8]. This study focuses on a specific diamond defect: the nitrogen-vacancy (NV) center, which has a nitrogen substitution in one carbon site and a vacancy defect in its adjacent site (Fig.1.2). This defect structure acts like a trapped electron with spin 1, resulting in atomic-like energy levels with underlying spin splittings (Fig.1.3). As shown in the energy level diagram, ground state NV-centers can be excited by 532 nm light and emit red light when relaxing from the excited state. One of the most important properties of NV-centers is their spin-dependent fluorescence: having three spin states ($m_s = 0$ or $m_s = \pm 1$), when relaxing from the excited state, NV centers with $m_s = \pm 1$ have a finite probability of going through a metastable state which does not emit any visible light, resulting in a weaker total photoluminances (PL) for $m_s = \pm 1$ NV-centers. Thus the amplitude of NV PL indicates different spin states of NV-centers. With no external magnetic field, the $m_s = \pm 1$ states have the same energy and can be excited from the spin-0 state by 2.87 GHz microwaves. When an external magnetic field is applied, the degenerate $m_s = 1$ and $m_s = -1$ spin states will split into two energy levels due to the Zeeman effect. As a result, the microwave frequencies required to excite $m_s = 0$ NV-centers to $m_s = \pm 1$ diverge from 2.87 GHz (Fig.1.4). The frequency difference is directly related to the magnitude of the applied magnetic field and is given by $2\gamma B_z$, where the NV gyromagnetic ratio $\gamma = 2\pi \times 28 GHz/Tesla$, and B_z is the magnetic field component that is parallel to the NV axis [9] [8].

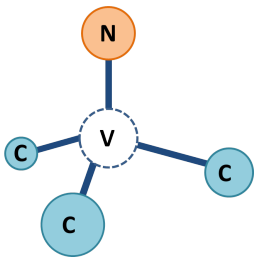

FIGURE 1.2: The NV-center in a diamond unit cell

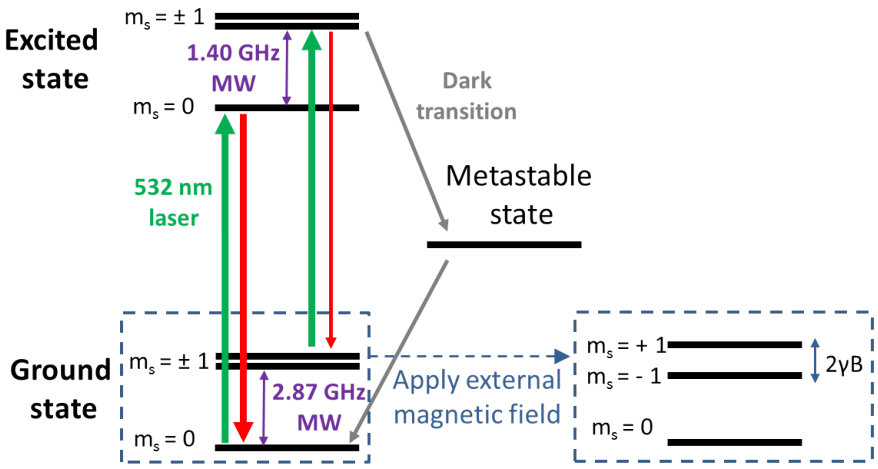

FIGURE 1.3: The energy level diagram of the NV-center in diamond. The ground state and excited state are similar to the electron energy levels in an atom. The $m_s = \pm 1$ states are degenerate at zero field and are split due to the Zeeman effect when external magnetic field is applied.

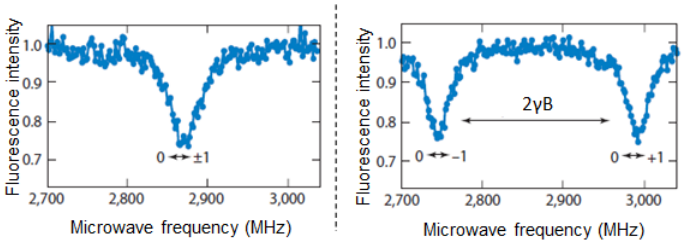

FIGURE 1.4: NV PL vs. microwave frequency, measured with continuous wave laser, with or without external magnetic field. The NV-centers are polarized to $m_s = 0$ state by the laser. When microwaves of 2.87 GHz are applied, some of the NV-centers are excited to $m_s = \pm 1$ states, resulting a decrement of NV PL. [9].

1.2.2 Optically Detected Ferromagnetic Resonance

An important property of a magnetic material is the magnetization–which describes the direction and density of the magnetic dipole moment of the material. Applying an alternating magnetic field on a ferromagnetic material exerts a torque on its magnetization and thereby causes the magnetization to process around the effective magnetic field (Fig.1.5) [10]. Uniform mode ferromagnetic resonance (FMR) is generated when the magnetic moments in the material process at the same amplitude and in phase. The FMR frequency of a ferromagnetic material can be described by the Kittel Formula $\omega_0 = \gamma[B_0(B_0 + \mu_0 M)]^{1/2}$ [11].

Typically, a resonance experiment setup consists of a static magnetic field H_0 and an field H_1 alternating at a certain frequency, usually generated by a microwave cavity or stripline. FMR is measured from the absorption of the microwaves by the ferromagnetic film: when the microwave frequency matches the ferromagnet's resonance condition, there will be a sharp absorption peak of the microwaves. Recently our group discovered that NV centers can also be excited from $m_s = 0$ state to $m_s = \pm 1$ states by the FMR of a nearby ferromagnetic material. The observed result wa a change in NV PL at magnetic fields or microwave frequencies away from NV resonance [4]. As shown in Figure 1.6, the two splittings at 1.40 GHz and 2.87 GHz at zero field correspond to the transitions from $m_s = 0$ to $m_s = \pm 1$ in the excited state and ground state respectively. Without the effect of ferromagnetic material, changing of NV spin states only happens at NV resonance, however, when NV-centers are located close to a ferromagnetic material–Yttrium Iron Garnet (YIG) in this case, their PL also changes when YIG is driven on FMR. The current understanding for this phenomenon is that the uniform mode FMR decays into spinwaves that are at NV resonant frequencies and thereby relaxes NV-centers [5] [4]. The study of this NV-FMR coupling is still ongoing, nevertheless, this phenomenon provides us a means to detect FMR by measuring NV PL. Thanks to its atomic size and sharp spin resonance, NV-center in diamond can be used to probe nanoscale local magnetic dynamics.

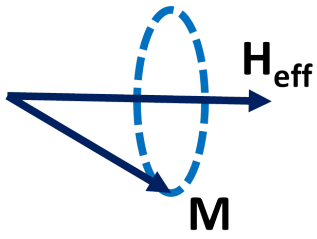

FIGURE 1.5: Ferromagnetic resonance (FMR). M is the magnetization of the material and H_{eff} is the effective field.

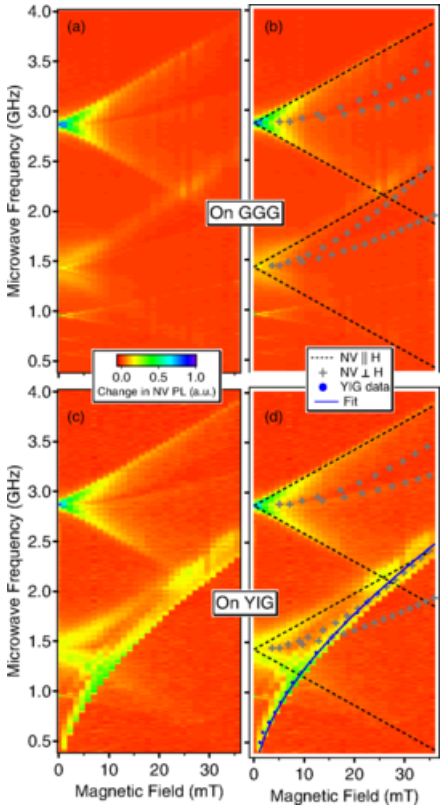

FIGURE 1.6: NV PL change while its nearby YIG film undergoes FMR. The two splittings at 1.40 GHz and 2.87 GHz indicate NV spin transition at the ground state and excited state. The FMR causes decrements of NV PL at frequencies far from the NV resonant frequencies. [4]

1.2.3 Surface Acoustic Waves

Surface acoustic waves (SAWs) have recently been considered an alternative way of drive FMR. SAWs are generated due to the change of strains of an elastic material and travel on the surface of the material. SAWs travel at the speed of sound. According to the relation between wavelength and speed $v = \lambda f$, where v is the speed that the wave travels at, λ is the wavelength, and f is the frequency, at the same frequency, SAWs have wavelengths that are approximately a million times shorter than electromagnetic waves. Their significantly shorter wavelengths allows electronics to be designed in much smaller sizes [7]. Moreover, being generated by electric field instead of current, SAWs avoid the energy loss due to electron flow, thus increase the device efficiency and can be used for low-power applications [6].

For acoustically driven FMR (ADFMR), SAWs generate elastic stains on the ferromagnetic material, and the anisotropy of the ferromagnetic material changes due to the magnetostriction, a magnetic property that describes the relation between the elastic deformation of a material and its anisotropy. In this experiment, the magnetostrictive ferromagnetic film is directly deposited on a piezoelectric substrate, and the SAWs carried by the substrate generate elastic strains on the ferromagnetic film and thereby drive FMR.

1.3 Methodology

1.3.1 The ADFMR Device

An ADFMR device used in this experiment is shown in Figure 1.7. A ferromagnetic film (Ni or Co) of size 1.5 mm $\times$ 0.5 mm is deposited on the piezoelectric substrate (lithium niobate). SAWs are generated by a set of interdigitated transducers (IDTs), which transform microwaves into SAWs. The IDTs are designed to transform microwaves only at its odd-numbered harmonic frequencies,

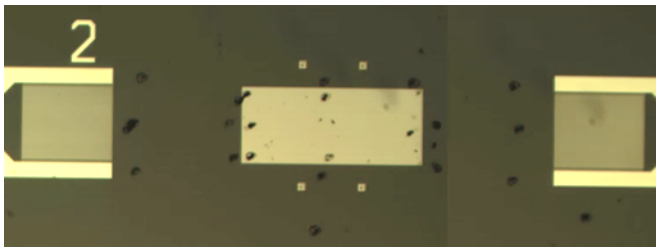

FIGURE 1.7: The ADFMR device with NV-diamonds. A ferromagnetic film (Ni or Co) is deposited between two IDTs, which transform input microwaves into SAWs. NV-diamonds are placed at various locations on the device surface, and their fluorescence is measured.

which are determined by the IDT's geometry. In this experiment, IDTs with a fundamental frequency of 287 MHz are used, which means that the IDTs transmit electrical signals at frequencies of 861 MHz, 1429 MHz, etc. Notice that the harmonics of each IDT can vary lightly ($\pm$ 5 MHz) and should be tested by taking field sweeps with no external magnetic field. The power loss from the microwave input to output is approximately 15 dBm, however, the loss of SAWs between the IDTs is as low as 0.1%.

NV-diamonds are deposited on the surface of the ADFMR device by dropping small droplets of NV-diamond suspension using glass needles. We choose to use suspension instead of powder to obtain a relatively uniform distribution of the NV-diamond on the device surface. The detailed procedure of depositing NV-diamonds on the ADFMR device can be found in Appendix A.

1.3.2 Experimental Setup for Continuous Wave ADFMR

A set of IDTs on the ADFMR device is wirebonded to SMA connectors for microwave input and output. Typically we generate 21.5 dBm microwaves from the microwave generator and use a 2 dB attenuator to avoid high power reflections gping back into the generator. Subtracting the power loss at the IDTs (7.5 dBm each), roughly 12 dBm microwaves are transformed into SAWs, and roughly 4.5 dBm microwaves are output at non-FMR frequencies. An external magnetic field is applied in-plan at an angle of 45 degrees relative to the SAW transmission direction (maximum

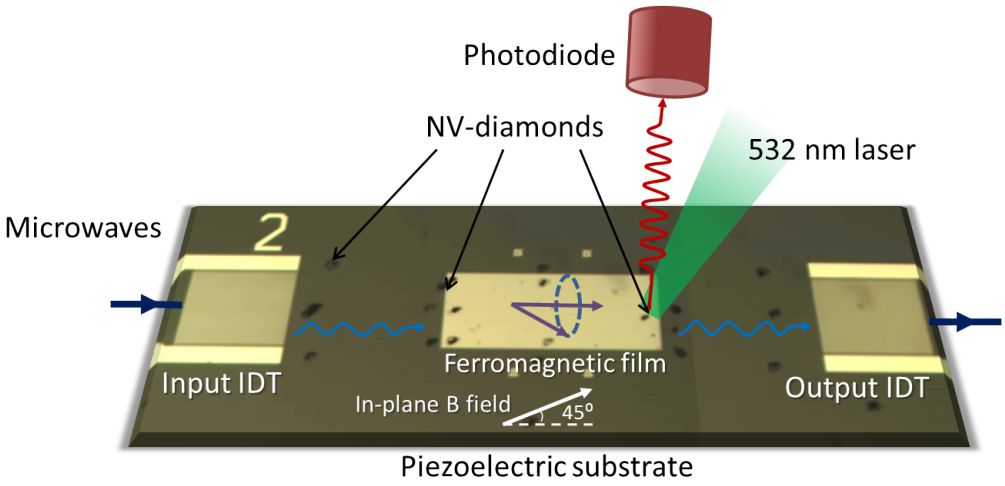

FIGURE 1.8: Experimental setup for the ADFMR experiment. The input IDT transform microwaves into SAWs which drive the FMR of the ferromagnetic film. The transmitted SAWs are converted back into microwaves and are measured by the output IDT. An in-plane magnetic field is applied to maximize the SAW absorption. NV-diamonds are deposited at different locations on the device surface, and their fluorescence is collected by a photodiode.

absorption angle [6]) in-plane with the ADFMR sample. The electromagnet supplies magnetic field up to ∼35.8 mT at the sample location using a 6 V power supply. Higher voltage (∼12 V) can be used for short-time field sweeps, but should not be applied to the magnet continuously to avoid magnet overheating. The voltage-field conversion is calibrated by placing a Hall probe at the sample position and has an error within ± 10%.

The input microwaves are transformed into SAWs through the IDT and the piezoelectrical substrate (lithium niobate). SAWs excite the ferromagnetic film to its FMR due to magnetostriction, and the FMR is detected both through the electrical transmission and NV PL change. We perform two kinds of measurements for FMR detections: sweeping microwave frequency at a fixed magnetic field (frequency sweeps) and sweeping magnetic field at a fixed IDT harmonic frequency (field sweeps). We modulated the input microwave, and the output electrical and optical signals are collected with two lock-in amplifiers. When FMR is reached, we expect absorption troughs on the electrical transmission and peaks on NV PL change.

We deposited NV-diamonds at different positions on the sample for control measurements as well as investigating local FMR, i.e. spatial dependence. However, since the morphology of each NV-diamond spot is different from each other, the NV PL change can be varied not only due to the sample position, but also the coupling between NV-diamonds and the ferromagnetic film.

More experimental details and tips can be found in Appendix A.

1.3.3 Experimental Setup for Pulsed ADFMR Measurements

Depending on the quality of the IDTs, some of the input microwaves will not be transformed into SAWs, but directly moving through the air. We designed a pulsed ADFMR experiment to eliminate the effect of these spurious microwaves. When a microwave pulse is sent in from the input IDT, the output signal is shown in Figure 1.9, in which the first small peak correspond to the spurious microwaves, the large peak corresponds to the SAWs, and the second small peak corresponds to the reflection of SAWs from the output IDT. The time difference between the microwave and the SAW peaks is a result of the different velocity the waves travel at and is determined by the distance between the two IDTs($\sim$800 ns in this case). The second microwave peak following the SAW peak shows up due to the reflection of the output IDT and is located halfway between the two pulses.

In this experiment, three pulses are generated: the input microwave pulse (excitation pulse), the laser pulse, and the detection pulse. An example is shown in Figure 1.11, in which the pulses are:

TABLE 1.1: Pulsed ADFMR example input pulses

Pulse	Initial delay (μs)	Width (μs)	Delay (μs)	Frequency (MHz)
Microwave	0	0.8	4.2	0.2
Laser	1.6	1.9	0.6	0.4
Detection	1.6	0.2	2.3	0.4

Excitation microwave pulse: To maximize the signal, we want to maximize the duty cycle of the excitation microwave, however, to avoid overlapping of the spurious microwave and SAW, the width of the pulse should be no longer than the SAW delay. In this case, we use a pulse width of 800 ns. The delay time of the excitation pulse is determined by the duration of the SAW, which is approximately 1.7 μs. To measure the NV PL change, the microwave pulses should have a different frequency than the laser pulse, and we choose to send in microwave pulse every alternate cycle, which gives a frequency half as the laser pulse frequency, therefore the total delay of the pulse is 1.7 + 2.5 = 4.2 μs.

Laser pulse: The laser pulse has two functions: the first 200 ns overlaps with the detection pulse for optical readout, and the pulse as a whole polarizes the NV-centers to $m_s = 0$ state. The laser pulse is set to be on as the detection pulse is on, and last until the beginning of the SAW pulse. The delay time of the laser pulse is set to give a frequency twice as the microwave pulse.

Detection pulse: The detection pulse decides when the optical and electrical signals are detected. Its width can be adjusted to maximize the signal as long as the frequency is the same as the laser pulse. An initial delay is set so that the detection pulse covers the peak of the SAW pulse and NV PL change.

*** Remaining issues:** In this experiment, all electrical transmission signals are obtained at the output IDT, however, the SAWs affecting on the ferromagnetic film should have different delay times. Moreover, these pulses were designed to have the same frequency first, and then the microwave pulse was turned off every other cycle. There might be alternative ways to design the pulses such that the microwave and detection pulses can have higher duty cycles.

The microwave and detection pulses are sent in three switches: one is between the microwave generator and the sample, one is between the output IDT and the lock-in for electrical signal, the last one is between the photodiode and the lock-in for optical signal. The pulses are generated with an NI DAQ and a pulser, and the details can be found in Appendix A.

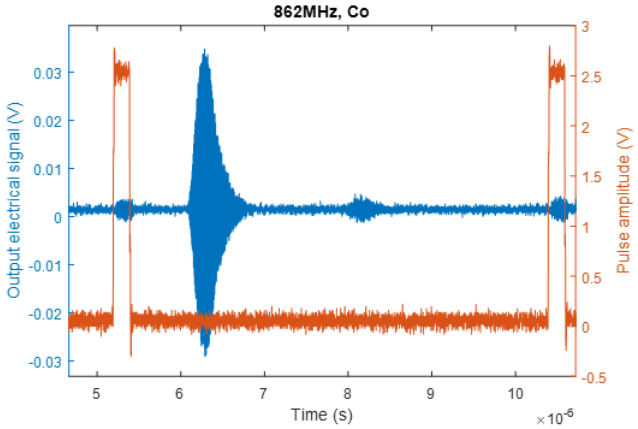

FIGURE 1.9: Electrical transmission signal for pulsed microwaves. Red = input microwave pulse; blue = transmitted electrical signal. The first small peak after the input pulse indicates the spurious microwave. The large peak and the second small peak indicate the SAWs and their reflections respectively.

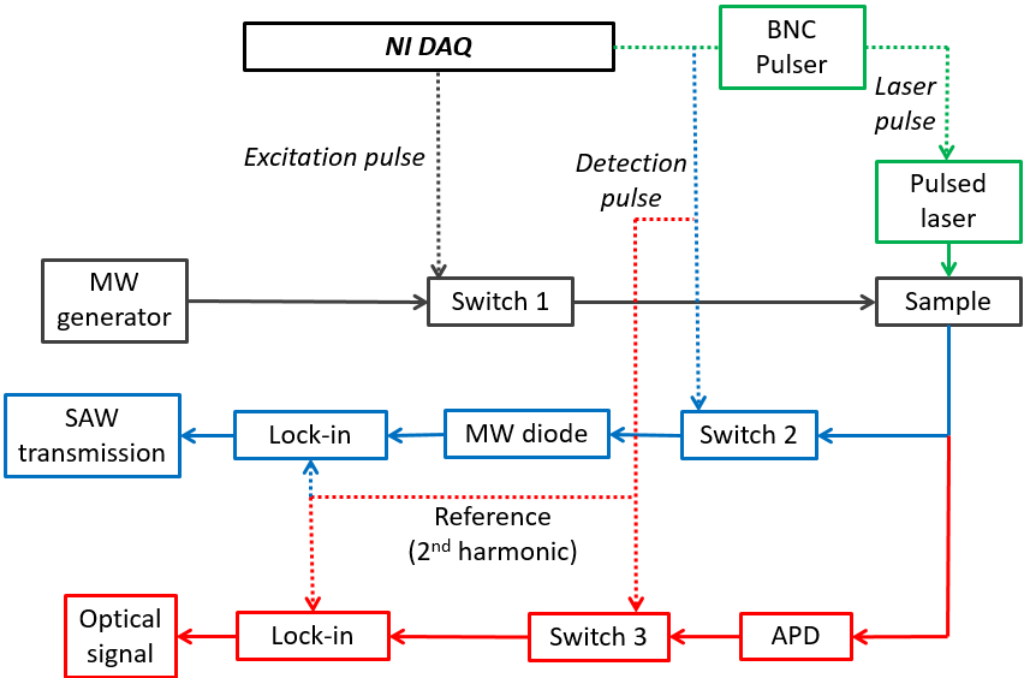

FIGURE 1.10: Block diagram for the pulsed ADFMR experiment.

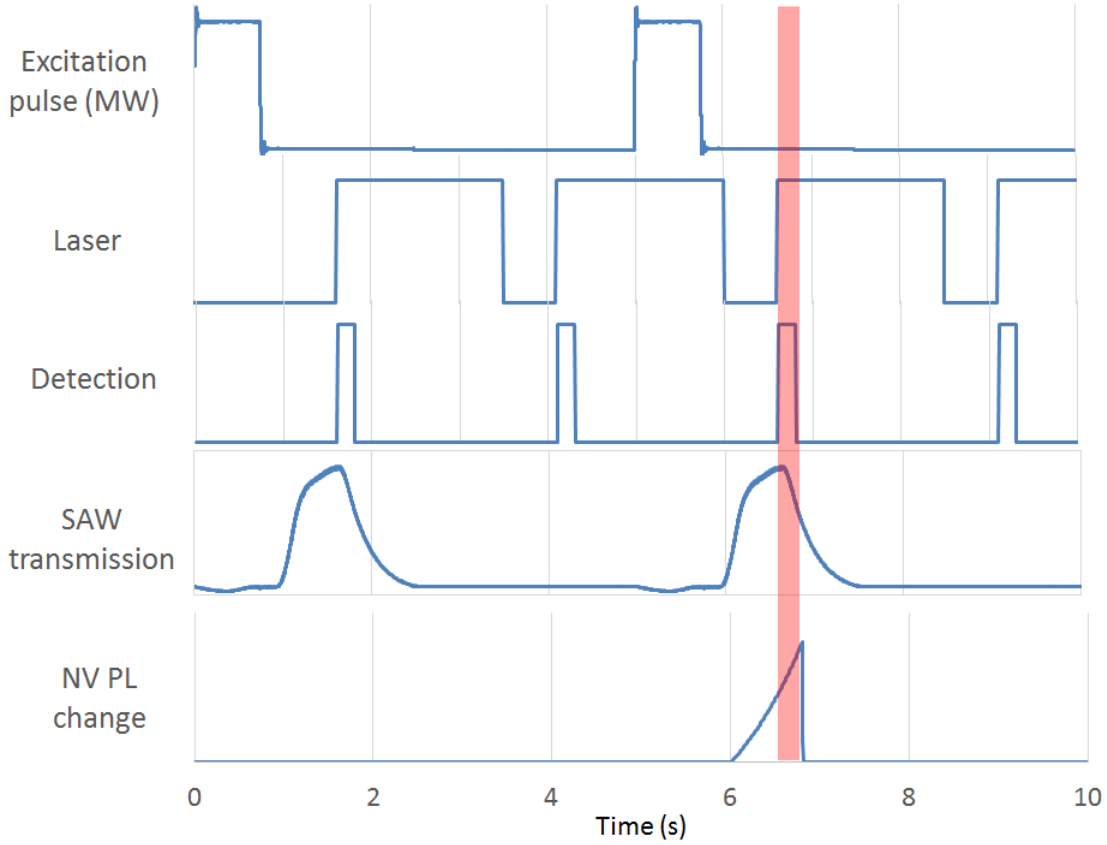

FIGURE 1.11: Pulses used in the pulsed ADFMR experiment. Pulses are generated for the excitation microwave, the laser, and the detections. Lock-in amplifiers are used to measure the output signals with a reference modulation same as the excitation microwave.

1.4 Results and Discussion

We tested and compared samples deposited with different ferromagnetic films (nickel and cobalt), as well as a controlled sample with no ferromagnetic film. We obtained multiple field and frequency sweeps under different conditions and as different NV-diamond positions.

1.4.1 Frequency Dependence

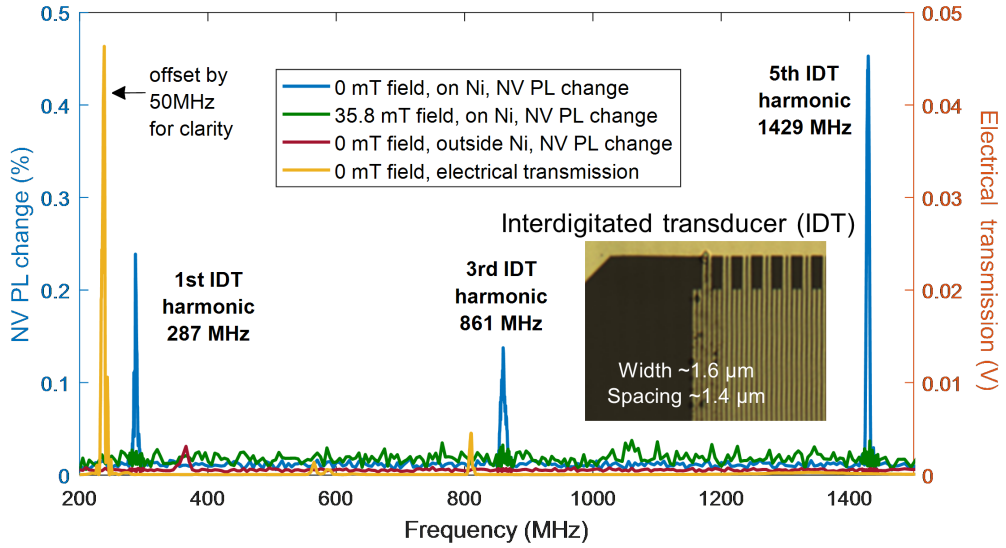

FIGURE 1.12: Frequency sweeps on Ni sample. Electrical signal peaks can be observed at the 1st and 3rd IDT harmonics, whereas the peak at the 5th harmonic is to small to be seen. The NV PL change peaks at the 1st, 3rd, and 5th IDT harmonics. The IDT harmonic frequency is decided by its finger width and spacing. An image of the IDT fingers is also shown.

The IDTs are designed to only transmit microwaves at its odd-number harmonics. For the devices used in this experiment, the fundamental IDT harmonic is at ∼287 MHz, and the 3rd and 5th harmonics are at ∼861 MHz and ∼1429 MHz. Figure 1.12 shows the electrical transmission and NV PL change at frequencies from 200 MHz to 1500 MHz. For Ni and Co, the FMR occurs at small

magnetic field (less than 5 mT) at the IDT harmonics, therefore the FMR can still be detected at zero-field. Electrical transmission and NV PL change are measured at zero magnetic field. We can observe that the transmission decreases significantly at high frequency, and the peak at 1429 MHz can hardly be seen. On the other hand, the NV PL change at zero-field is smaller at 861 MHz comparing to at 287 MHz, but the peak at 1429 MHz has the maximum amplitude. One possible explanation for this is that the 5th harmonic is very close to NV excited state resonant frequency (1.40 GHz), and the NV-centers are excited to $m_s = \pm 1$ by the FMR uniform mode directly, instead of the spinwaves it decays into. The NV PL change is also measured at high magnetic field (35.8 mT), which is far from the FMR field of Ni and Co. Since there is no FMR effect, the NV PL change peaks disappear. Another control measurement is done by measuring NV PL change at NV-diamond spot outside the ferromagnetic film. Due to the lack of ferromagnetic material, FMR does not affect NV PL in this case either, thus no NV PL change peaks.

*** Remaining issues:**

1. The small peak observed of NV PL change outside Ni (red line) at approximately 360 MHz is not noise. The data were averaged from 20 repetitions, and this peak has also been observed on another Ni ADFMR sample. Further investigations of this peak are needed.

2. The amplitude of the NV PL change peaks are not very consistent and is highly dependent on the position of the laser spot, i.e. the quality of coupling between the NV-diamonds and the ferromagnetic material at this position. The NV PL change at 861 MHz usually, but not always, has smaller amplitude than the other two peaks.

3. The values of the electrical signal might be inaccurate due to the damaged microwave diode.

1.4.2 Field Dependence

We held the microwave frequency at the IDT harmonic frequencies and swept magnetic field. The troughs of the electrical transmission indicate that the ferromagnetic film has reached its FMR.

The NV PL response can be observed clearly on the 287 MHz and 861 MHz sweeps, where two peaks occur at the same time as the electrical transmission decreases. At 1429 MHz, however, a larger peak occurs at 0 field, and the two FMR peaks merge together, forming a single peak with fine features at its maximum. The zero-field peak at 1429 MHz consist with the NV excited state resonant condition, and NV-centers might be directly excited by the FMR uniform modes in the ferromagnetic material.

Comparing Ni and Co, the electrical absorption at FMR is significantly larger on Ni, especially at 862 MHz. The magnitude of NV PL change peaks, however, do not show a correlation with the electrical absorption–at lower frequencies (287 MHz and 861 MHz), the NV PL on Co changes more than on Ni, whereas at 1429 MHz, the NV PL change peak on Ni is almost one order of magnitude larger than on Co. The features at the peak maximum is also less identifiable on Ni.

*** Remaining issues:**

1. The irregular electrical transmission between the two FMR troughs is related to the orientation of the magnetic field, i.e. the out-of-plane field. If the sample position is adjusted well enough that the out-of-plane field is very small, this effect should be eliminated.

2. The two peaks of NV PL change are not always observable. Some measurements on the same sample only show one peak at zero-field. Further experiments should be done to obtain consistent measurements.

3. The NV PL change has an linear offset at 287 MHz and 861 MHz. This offset is reduced but not eliminated when we switched from Adamas NV-diamond suspension to water suspension.

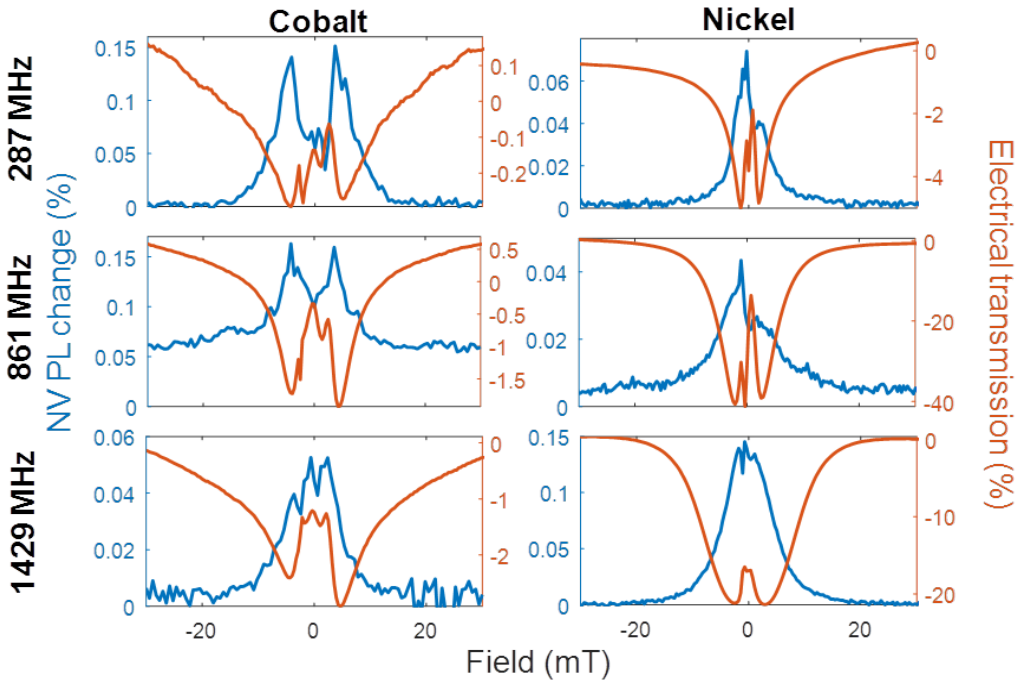

FIGURE 1.13: Field sweeps on Ni and Co sample at IDT harmonic frequencies. A correlation between the NV PL change and the electrical absorption can be seen. The NV PL change has two peaks at 287 MHz and 861 MHz, whereas at 1429 MHz, the two peaks merge together and a third peak at zero field appears.

1.4.3 Spatial Dependence

As mentioned int he Methodology section, NV-diamonds are deposited at various positions on the device surface. The measurements were performed on a Ni ADFMR sample for which the IDTs are slightly damaged and gives high spurious microwave at high frequency. Shown in Figure 1.15, the sharp peaks at ∼287 MHz and ∼861 MHz are transmitted SAWs, and all the irregular peaks are results of spurious microwave. We measured the NV PL change at different positions, and three representative ones are plotted in Figure 1.14. At 287 MHz and 861 MHz, where FMR is the only excitation source, only the NV-diamonds on the Ni film (yellow spot) have NV PL change. At 1431 MHz, NV-diamonds that are not on the Ni film (blue and orange) also have PL change, and NV

PL change at the blue position–which is closer to the input IDT–higher than the orange position. These two peaks are clearly not due to FMR and might be a result of the spurious microwave excitation of NV at ground state: the frequency sweep (Fig. 1.15) does show a considerable amount of microwave at 1431 MHz, and the larger peak at the blue position indicates that the microwave is stronger closer to the input IDT. The field sweep at 2875 MHz, the NV ground state resonant frequency, further confirmed that NV-centers can be excited by the spurious microwave directly. The peak amplitudes decreases for NV-centers further away from the input IDT. Considering the electrical transmissions are measured at the output IDT, the actual microwaves acting on the NV-diamonds are possibly stronger than shown in the frequency sweeps.

*** Remaining issues:**

1. Again, NV PL change is highly dependent on the coupling between NV-diamonds and the device surface. A slight motion of the sample can lead to a huge change of the PL.

2. There are some NV PL change signals for the two off-Ni positions, shown as small bumps on Figure 1.14 at 287 MHz and 861 MHz. This could be caused by the chemicals in the Adamas NV-diamond suspension, but it is seemingly sensitive to magnetic field.

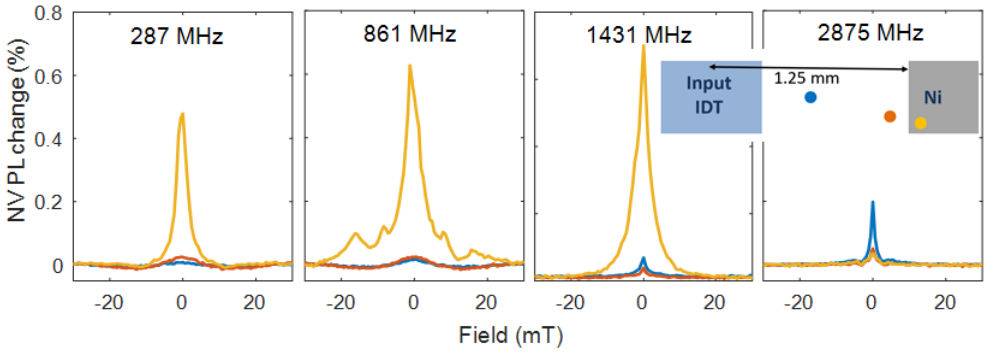

FIGURE 1.14: Field sweeps on Ni sample at different NV-diamond positions. The effect of the spurious microwave can be observed at 1431 MHz and 2875 MHz. Field sweeps at 2875 MHz show that the microwave effect increases at positions closet to the input IDT.

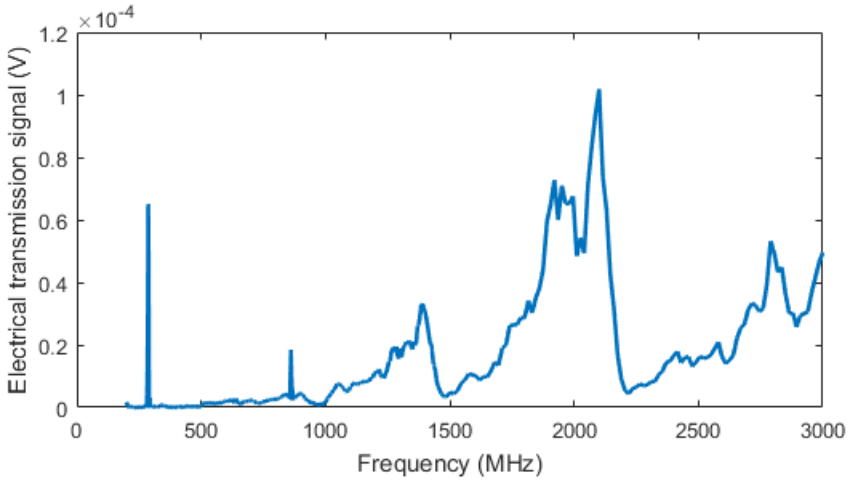

FIGURE 1.15: Frequency sweeps on Ni sample, electrical transmission signal. The two sharp peaks at 287 MHz and 861 MHz are SAWs, and the irregular signals indicate spurious microwaves.

1.4.4 Pulsed ADFMR

We tested the output signal (optical and electrical) strength at different detection pulse frequencies. The excitation microwaves are modulated at 100 kHz, 50% duty cycle. We vary the detection pulse

frequency from 100 Hz to 1.82 MHz, all at 50% duty cycle. The results are shown in Figure 1.16. We can see that both optical and electrical (S12) signals keep constant until 100 kHz, which is exactly the input microwave frequency. When the detection pulse frequency exceed 100 kHz, the pulse width is not long enough to cover the entire microwave pulse, thus only partial signals are detected, resulting in a decreasing signal amplitude. The higher the detection pulse frequency is, the smaller the pulse width, and less signal is detected.

The detected signal strength also depend on the relative phase of the detection and excitation pulses. Figure 1.17 shows the transmitted electrical signal (S12) for different detection pulses, varying the initial delay time. The detection signal goes to zero when the detection pulse is completely out of phase with the transmitted signal. Although smaller duty cycle detects less signal, the pulse edge is sharper than the large-duty-cycle pulses.

Due to time and equipment limitations, we were not able to perform much measurement using the pulsed setup. The signals detected are significantly weaker than the continuous wave (CW) measurements. With pulses listed in Table 1.2, a small peak is observed at ~287 MHz on the Co sample by taking averages from 20 sweeps (Fig. 1.18). Measuring ADFMR with pulsed microwaves should be approachable if we can reduce the noise and further amplify the optical signals.

TABLE 1.2: Pulsed ADFMR input pulses

Pulse	Initial delay (μs)	Width (μs)	Delay (μs)	Frequency (MHz)
Microwave	0	0.8	9.2	0.1
Laser	0.6*	1.9	3.1	0.2
Detection	1.6	0.5	4.5	0.2

* There is a 1 μs internal delay from the laser source, therefore the total initial delay is 1.6 μs.

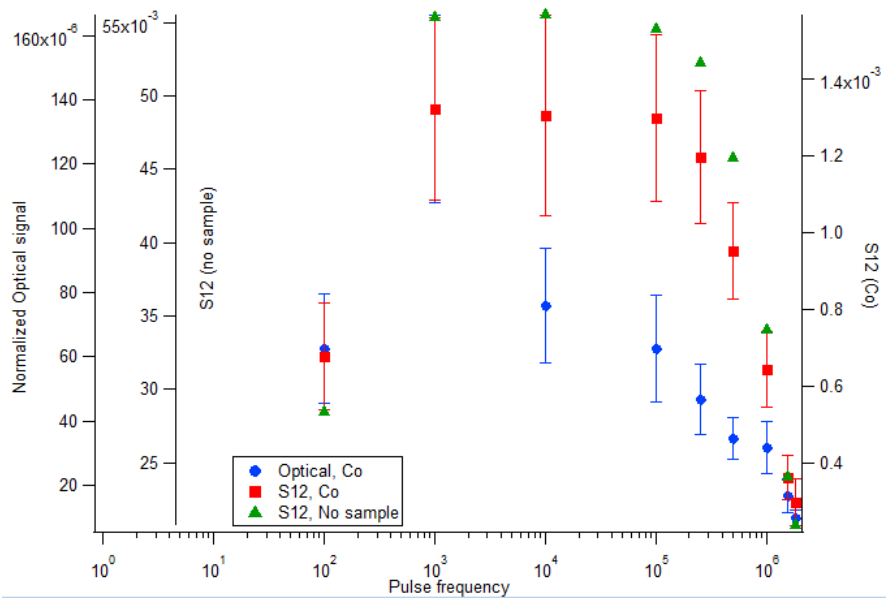

FIGURE 1.16: Output signal amplitude of 861 MHz input microwaves modulated at 100 kHz (50% duty cycle), varying the detection pulse frequency (50% duty cycle).

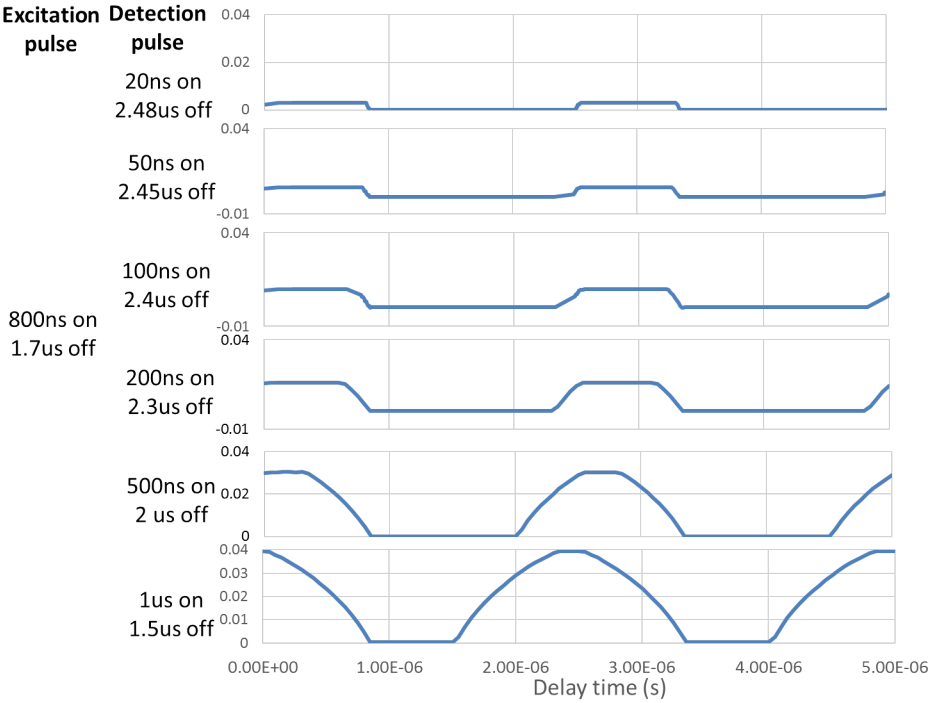

FIGURE 1.17: Electrical transmission signal amplitude of 861 MHz input microwaves modulated at 400 kHz (32% duty cycle), varying the detection pulse duty cycle and initial delay time.

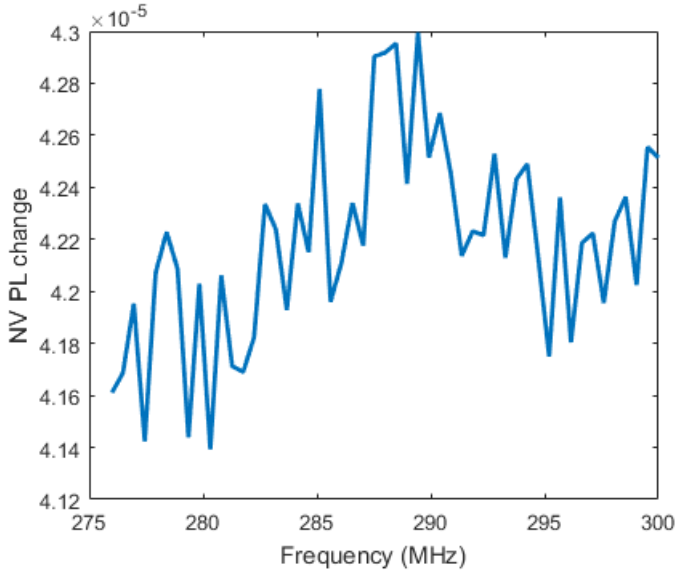

FIGURE 1.18: Frequency sweep on Co sample with the pulsed ADFMR setup. Taken from 20 averages. A small peak can be seen at around 287 MHz.

1.5 Conclusion

We successfully measured ADFMR on nickel and cobalt using NV-centers. A general protocol of depositing NV-diamonds on the ADFMR devices is developed. We performed frequency and field sweeps at multiple positions on the ADFMR samples and observed peaks of NV PL change when the ferromagnetic film reaches FMR. The PL intensity is tested to be very sensitive to the distance between NV-diamonds and the ferromagnetic film. We compared ADFMR on Ni and Co and found that although Co has a larger magnetostriction, with the same microwave frequency, it required higher magnetic field to reach FMR. The electrical absorption of Co is also higher than Ni in an order of magnitude, whereas the NV PL changes are in the same order of magnitude on both materials. The FMR-driven NV PL change disappears when the NV-diamonds are outside the ferromagnetic film or when higher magnetic field is applied. We have also observed the effects of spurious microwaves on NV-diamonds: the spurious microwaves are able to drive NV resonance directly at $\sim$1.40 GHz and $\sim$2.87 GHz and their intensity decreases at positions further aways from the input IDT. We eliminated the spurious effects by applying pulse microwaves and pulsed detections. The resulting signals are smaller than the continuous wave measurements by two orders of magnitude and can hardly be identified from the background noise.

Chapter 2

Developing a Spatially Scannable Diamond Probe for Sensitive Nanoscale Magnetometry and Spectroscopy

2.1 Introduction

Mapping nanoscale magnetic fields with high spatial resolution has always been a major research aim in various disciplines, from magnetic resonance imaging (MRI) for medical diagnosis, to magnetic hard drive design and manufacture. Magnetometry is the technique of measuring and imaging magnetism. Current magnetometry techniques, e.g. superconducting quantum interference devices (SQUIDs) and magnetic force microscopy (MFM) are not ideal for providing high magnetic sensitivity and high spatial sensitivity at the same time [3]. NV-centers in diamond are recently considered a potential alternative solution to building nanoscale magnetometers. Our previous study on ADFMR shows a dependence of NV-center fluorescence on its position relative to the ADFMR device. Mapping the ADFMR device with NV-diamonds at an arbitrary position with more accurate controls will allow us to further study the spatial relations between NV-centers and FMR. The goal of this project is to develop a spatially scanned nanodiamond probe, which

will enable imaging of magnetic fields at nanoscale with nanotesla range sensitivity, by attaching nanodiamonds containing NV defects to the tip of an atomic force microscope (AFM) cantilever. The attachment was achieved by manipulating the AFM scan modes and parameters during the scanning of NV-diamonds deposited on silicon substrate. We have developed a microscope-based setup to image fluorescence of NV-diamonds under laser excitation and have successfully attached multiple NV-diamonds to an AFM cantilever tip. Several measurements have been done to characterize the NV-diamonds attached cantilever. Future study will be focused on developing single NV-diamond attached scanning probe, as well as performing magnetic measurements with multiple NV-diamonds attached probe.

Multiple nanodiamonds were successfully attached to an AFM tip by scanning an AFM tip charged by poly-l-lysine over an ensemble of nanodiamonds dispersed on a silicon substrate. The nanodiamoands picked up by the AFM tip have been characterized by optical fluorescence, optically detected magnetic resonance and scanning electron microscopy. This NV-diamond probe can be potentially used to map NV PL change over the ADFMR device.

2.2 Background

2.2.1 Atomic Force Microscopy

Atomic force microscopy (AFM) is a scanning technique that has a resolution in nanoscale. AFM scans the sample surface morphology with a mechanical probe with tip radius as small as several nanometers. The basic mechanics of the AFM is shown in Figure 2.1. The scanning probe is brought in contact with the surface of the sample and is scanned over the desired area. Topological features on the sample surface result in motions and change of force on the probe [12]. The motion of the cantilever due to the force is detected by its reflection of a laser beam. Because of the interaction between the AFM probe and the sample surface, AFM can also be used to perform

nanomanipulations. Two of the most common AFM scanning modes are contact mode and taping mode. In contact mode, the AFM probe tip is in contact with the sample during the entire scanning, and the sample morphology is obtained by measuring the deflection of the probe cantilever. In tapping mode, the probe is oscillating at or very close to its resonance frequency, and the change of the oscillation amplitude is detected and used to derive the topological features of the sample. The perturbation to the sample is much smaller using tapping mode than contact mode, therefore tapping mode can be applied to unstable samples such as powders and soft materials.

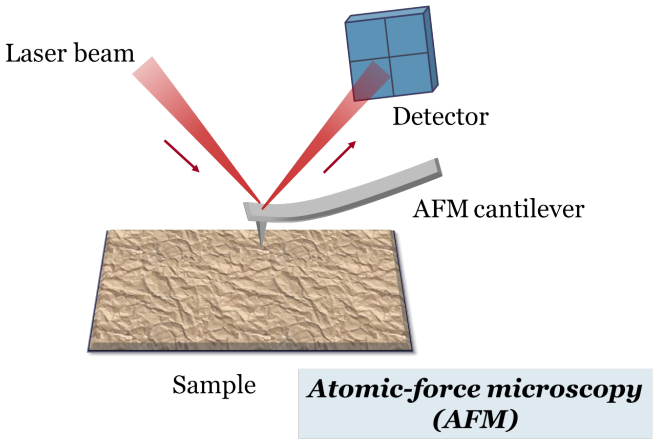

FIGURE 2.1: The basic mechanism of atomic force microscopy (AFM). The AFM probe is in contact with the sample surface, and the deflection of the AFM cantilever is measured with a laser beam.

2.3 Methodology

We use the Adamas NV-diamond suspension (nanodiamond radius = 100 nm) to deposit NV-diamonds on silicon substrates, and then attach the NV-diamonds to an AFM probe tip by scanning a small region of the sample that contains a certain amount of nanodiamonds using AFM contact mode.

2.3.1 Depositing NV-diamonds on Si Substrates

To obtain different dispersions of the NV-diamonds, we diluted the 1 mg/mL Adamas NV-diamond suspension by factors of 100, 10^3, 10^4 and 10^5 with distilled water. Silicon wafers were cut into 5 mm $\times$ 5 mm square pieces for use as substrates. The substrate was placed on a hotplate at a temperature of $\sim 270^oC$. The substrate was left on the hotplate for $\sim$5 minute to reach the equilibrium temperature, an then 5 μL of diluted NV-diamond suspension was obtained with a micropipette and dropped on the substrate. NV-diamonds were deposited on the Si substrate after the solvent was evaporated. The remaining NV-diamonds tend to concentrate and form multiple "rings" (Fig. 2.2).

We have also tried to use a spinner to spin the substrate while depositing NV-diamonds in order to obtain a uniform dispersion. Given multiply trials with various spin speed, however, we found that only a small amount of nanodiamonds remained on the substrate after spinning. Later AFM scans show that we are able to find dispersed or single NV-diamonds on a drop-deposited, unspinned sample, therefore the drop-suspension procedure is the best method so far finding dispersed single NV-diamonds.

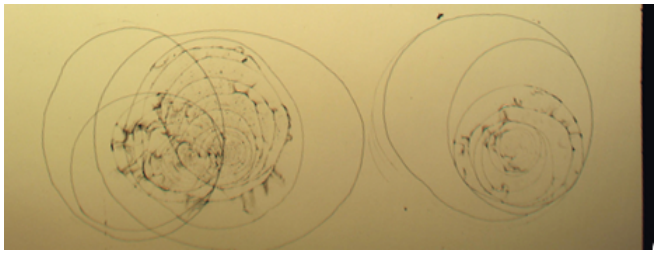

FIGURE 2.2: NV-diamonds deposited on Si substrate. 10 μg/mL NV-diamond suspension was used. The diameters of the outer most rings are approximately 1 mm.

2.3.2 Attaching NV-diamond to AFM Cantilever Tips

We attach NV-diamonds to the probe by using AFM contact mode scan a small area of the sample that was deposited with NV-diamonds. To reinforce the attachment, the tip of the probe was coated with poly-l-lysine, a positively charged polymer that increases the attraction between the probe tip and the negatively charged NV-diamonds [13] [14]. We first scanned the sample using AFM tapping mode and located a region with desired amount of nanodiamonds (usually an area less than $10 \times 10\ \mu m^2$). We then switch to the contact mode and scan the target area (Fig. 2.3), and some of the nanodiamonds in this area would attach to the tip of the AFM probe. After the nanodiamonds are attached to the probe, it is unlikely for them to fall off [15].

We also made attempts to attach a single NV-diamond to the probe tip. Using the same procedures, we were able to locate single NV-diamonds even on the most concentrated sample (10 μg/mL). We have also observed that the nanodiamond being moved after contact-mode scans, however, attaching a single NV-diamond to the probe tip still remains unaccomplished after numerous tries.

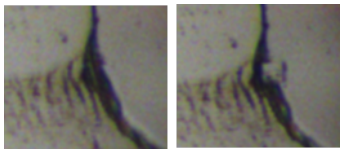

FIGURE 2.3: Optical image of NV-diamonds before (left) and after (right) AFM contact mode scanning of a $10 \times 10\ \mu m^2$ area. The nanodiamonds in the scanned region are clearly removed. The image width is approximately 0.1 mm. $10\ \mu g/mL$ NV-diamond suspension was used for this sample.

2.3.3 Optically Detected Magnetic Resonance of NV-centers

We modified an inversed microscope to measure the NV PL. Shown in Figure 2.4, a 532 nm laser beam is shot through a ND filter, reflected by two mirrors. The most collimated part of the beam is

then selected by an aperture, and finally sent into the microscope. In front of the microscope, there is a defocusing lens mounted on a flip mount. The defocusing lens allows us to adjust the beam size to observe NV-diamonds in a relatively large area (∼0.15 mm beam diameter) with relatively lower laser intensity, or focus down on a small point with higher laser intensity. In this case, we set up the defocusing laser when obtaining the NV-diamond PL on Si substrates (for example, second picture on Figure 2.8) and put down the lens when measuring the NV PL on the tip of a cantilever (Fig. 2.9, left column). Inside the microscope, the 532 nm laser beam is first reflected by a dichroic mirror, which reflects green light and transmit red light. The red NV fluorescence then passes through the dichroic mirror and a long pass filter, is reflected by a mirror, and focused on a photodiode. Figure 2.5 shows the locations of the electromagnet and the positioning stage in this setup. The electromagnet was used to supply the external magnetic filed and generates Zeeman splitting of the NV-centers. We used a 3-axis positioning stage and some 3D-printed parts to hold the AFM cantilever above the objective, where the laser beam was focused. A piece of thin wire (Fig. 2.6) was connected to an SMA connector an was held very close to the NV-diamond-covered AFM cantilever tip (seperation $\sim 350\ \mu m$, see Fig. 2.7). Microwaves were generated by running AC current through the wire in order to drive NV resonance. Modulating the input microwave at 1 kHz, the NV fluorescence was collected by the photodiode, and the change of NV PL was measured by a lock-in amplifier.

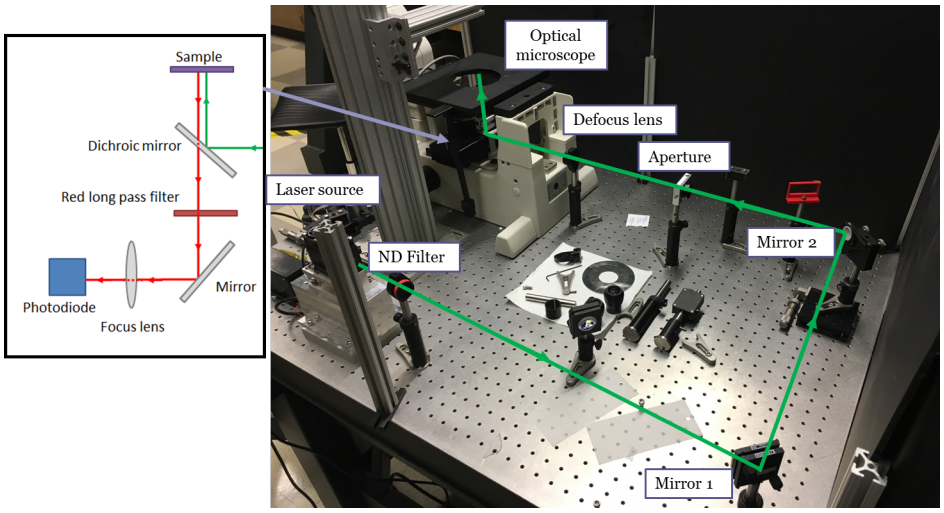

FIGURE 2.4: The Nikon setup used to measure NV PL. The setup consists of a inverted microscope, a defocus lens on a flip mount, several mirrors and filters, and a laser source. The inner structure of the microscope is shown next to the picture.

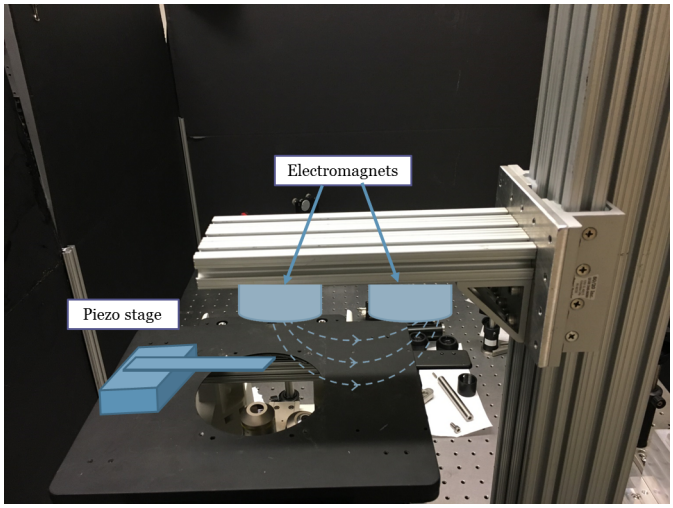

FIGURE 2.5: A picture shows the locations of the electromagnet and the positioning stage.

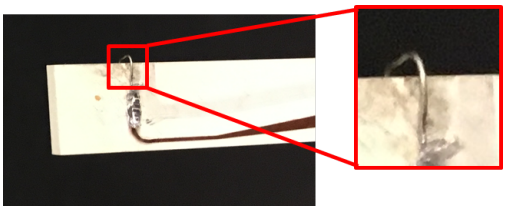

FIGURE 2.6: Thin wire used to supply microwaves.

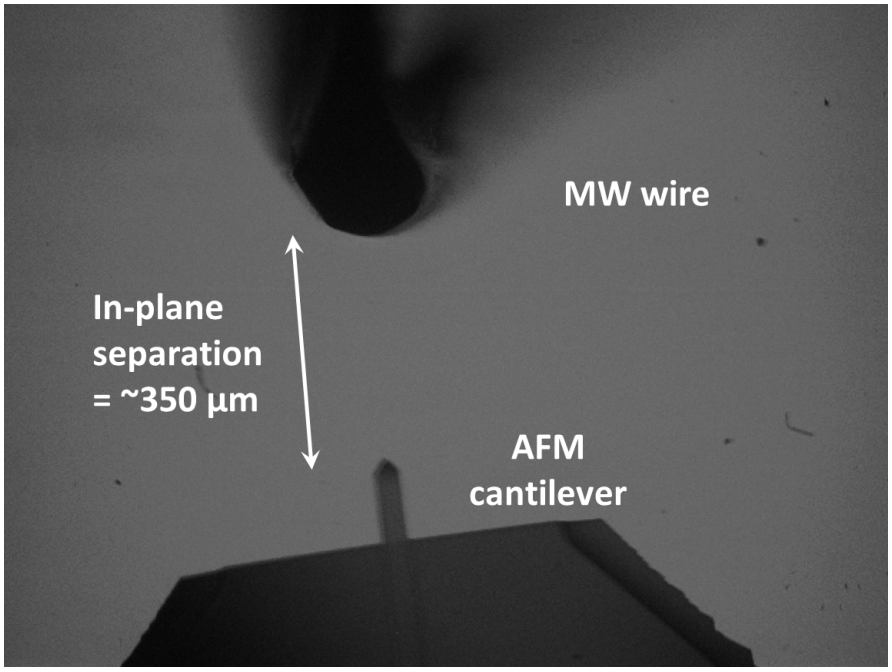

FIGURE 2.7: Microscopic image of the edge of a microwave wire and an AFM probe nearby.

2.4 Results and Discussion

We deposited NV-diamonds on silicon substrates with suspensions of different concentrations. The sample obtained from 10 μg/mL suspension was used since we were able to identify both single NV-diamonds and clusters with a large amount of NV-diamond. Shown in the AFM image in Figure 2.8, several single nanodiamonds can be seen close to the ring and in the bottom left corner.

We successfully developed five NV-diamonds-attached AFM probes, each with different amount of nanodiamonds. SEM images were taken on three of them, and one unused AFM probe for comparison. The results are shown in Figure 2.9. Comparing to the unused probe, the probe tip is clearly flattened during the contact-mode scanning, and a large amount of nanodiamonds accumulate on the side of the tip. We observed red fluorescence from the second probe, but the SEM image shows some layered structures that are unlikely to be nanodiamonds. Considering the suspension contains a small amount of organics to stabilize the nanoparticles, this layered structure could be organic residues which also fluorescent. The amount of nanodiamonds attached to the probe tip is proportional to the nanodiamond density at the area of scanning.

We took an ODMR spectrum on the NV-diamond probe that gives the strongest fluorescence, and the result is shown in Figure 2.10. A peak of NV PL change is clearly seen at around 2.87 GHz, which is the NV ground state resonant frequency. The ODMR spectrum further proved that NV-diamonds are attached to the AFM probe tip and the NV PL change is measurable.

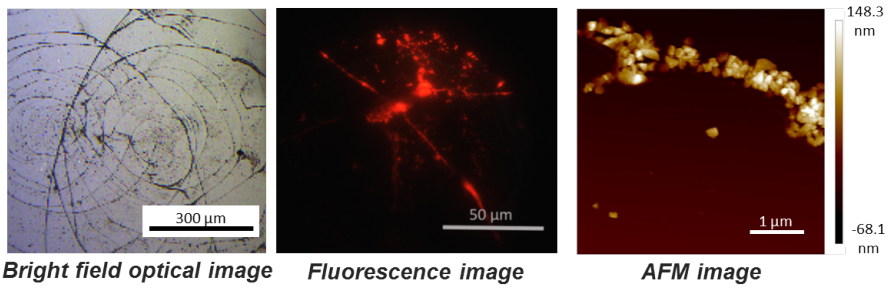

FIGURE 2.8: NV-diamonds dried from suspension drops on silicon substrate.

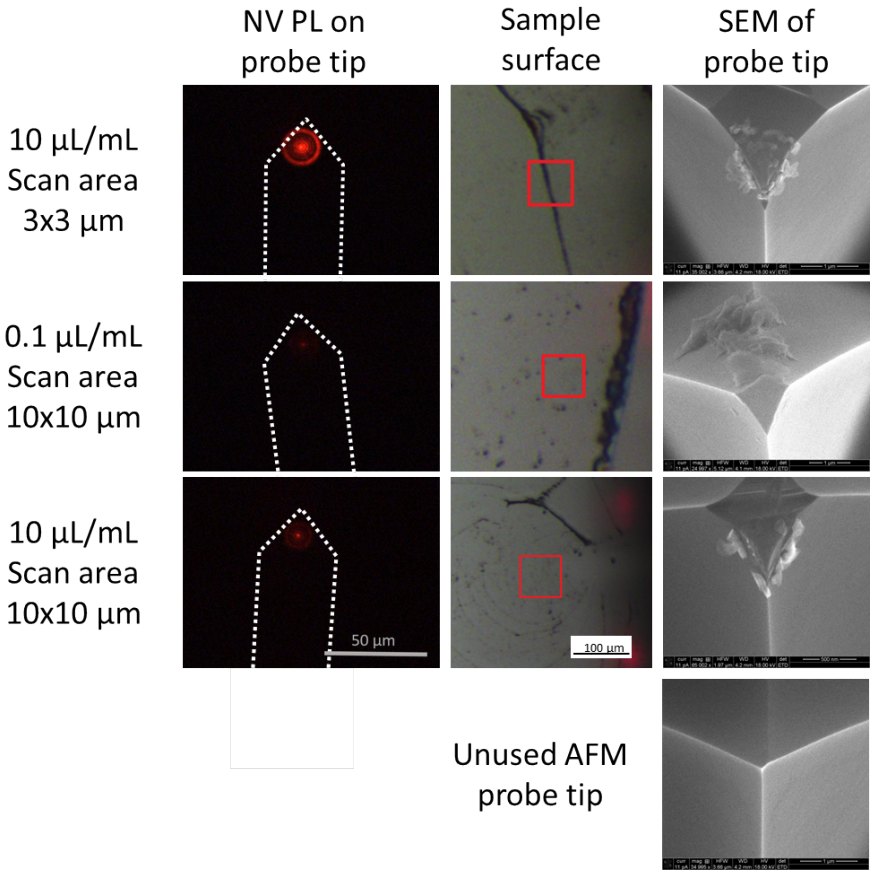

FIGURE 2.9: SEM and fluorescence images of an AFM cantilever before and after attached with NV-diamonds. The white dashed lines outline the probe. The red squares roughly indicate the region of scanning (not the exact scan area).

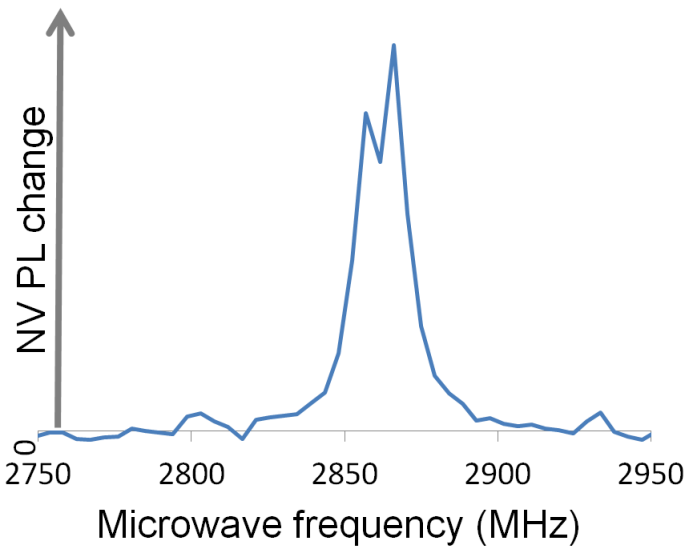

FIGURE 2.10: An ODMR spectrum taken from a NV-diamond-attached AFM probe at zero magnetic field. A peak can be seen at NV ground state resonant frequency (2.87 GHz).

2.5 Conclusion

We developed a general protocol to attach NV-diamonds to an AFM probe tip. Different amounts of NV-diamonds were attached to 5 AFM probes. The fluorescence image and SEM image of 3 selected NV-diamond probes were taken and compared. We have also built a experimental setup to measure the fluorescence and ODMR of small amounts of NV-diamonds. ODMR spectrum of NV-diamonds on an AFM probe was taken and shows a resonance at around 2.87 GHz, which consist with the NV resonant frequency in the ground state.

Appendix A

Detailed Experimental Procedures

A.1 ADFMR

A.1.1 Depositing NV-diamonds on the ADFMR device

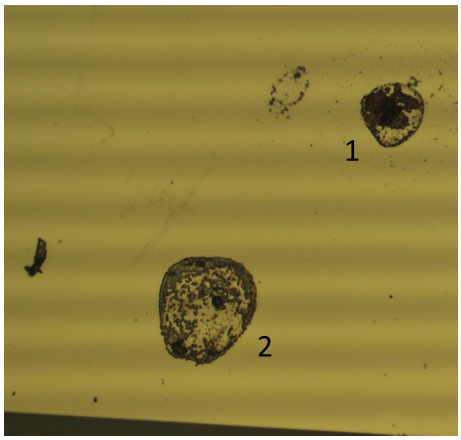

FIGURE A.1: NV-diamonds deposited on Ni pad on an ADFMR device.

NV-diamonds are deposited on the ADFMR device by dropping NV-diamond suspension drops at the desired locations. This deposition is performed under a long-working-distance microscope using hollow glass needles. Glass tubes with inner diameter of 0.7 mm are pulled into glass needles. The deposition procedures are the following:

1. Shake or sonicate the NV-diamond suspension.

2. Obtain $10\ \mu L$ NV-diamond suspension on a glass slide, immerse the tip of the glass needle into the suspension drop until liquid is sucked into the needle. A small portion of the needle tip might need to be removed by tweezers to allow the suspension flow in.

3. After obtaining the suspension in the glass needle, gently tap the needle tip at the desired location to leave small drops of NV-diamond suspension on the device surface. Multiple taps can be performed depending on the suspension concentration. The amount of NV-diamonds deposited at one spot should be enough to give a measurable signal, but should not be too much that the coupling between the NV-diamonds and the ferromagnetic film will be weaken due to the NV-FM separation. As shown in Figure A.1, Spot 1 gives enough PL to measure NV signals, but Spot 2 is not dense and uniform enough to obtain consistent, low-noise NV signals.

   (a) Notice that the amount of NV-diamonds deposited per tap depends on the surface material. It is usually easier to deposit NV-diamonds on the lithium niobate substrate than on the Ni or Co pad.

   (b) Also notice that the Adamas 1mg/mL NV-diamond suspension is easier to deposit than the water suspension, but the Adamas suspension contains chemicals that also gives optical signals.

4. NV-diamonds in suspension (especially for the water suspension) tend to accumulate on the glass needle tip. A small amount of NV-diamond accumulation could make the deposition easier, however, the accumulation might eventually lead to large clumps that end up on the surface and cannot be used to obtain optical signals.

5. Similar clumping is observed for the suspension drop on the glass slide. The nanodiamonds tend to accumulate on the edge of the drop, if a droplet is left for more than several minutes, it might not have as high of a concentration as it used to.

A.1.2 Tips for Using the Nikon Setup

1. **Sample positon**: To obtain a maximum in-plane magnetic field, the ADFMR sample should be placed below and parallel to the magnet and halfway between the center pole piece and one side pole piece (Fig.A.3). The vertical distance from the sample to the magnet is marked on the stand and should be kept constant. The relative position of the sample to the magnet should be adjusted by moving the magnet frame, since the sample position is determined by the laser spot, which cannot be changed without adjusting the optical alignments.

2. **Connecting the ADFMR sample**: The ADFMR sample is connected to two SMA flex cables, one on each side. The cables are taped down on the microscope stage. Since the optical signal depends strongly on the morphology of the NV-diamond spot, *motions of the sample should be avoided during measurements*.To minimize sample motions, wait until the SMA cables relaxed to a stable position before taking measurements. One could also design a 3-D printed part to fix down the sample.

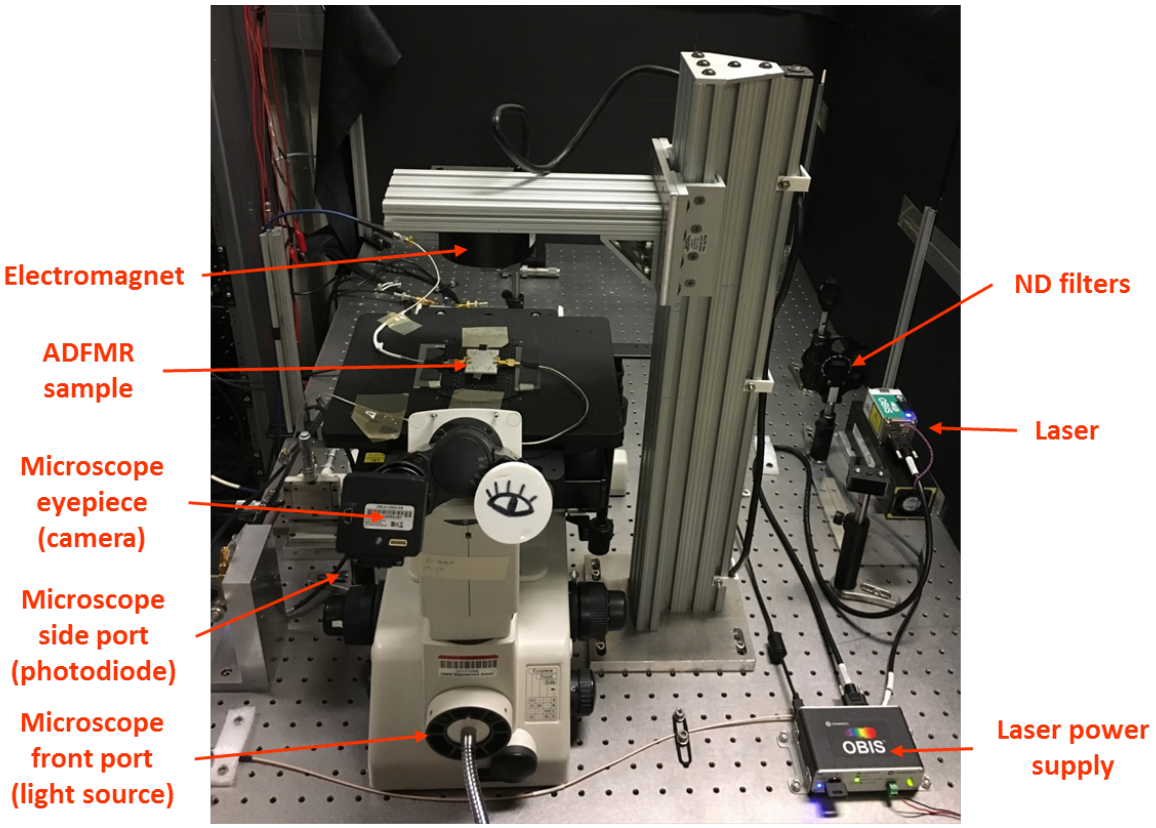

FIGURE A.2: Nikon setup for the ADFMR experiment

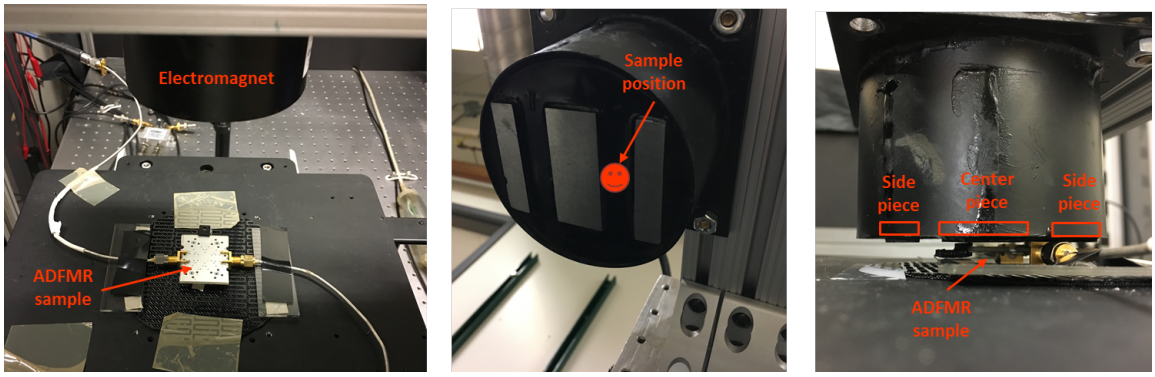

FIGURE A.3: ADFMR sample position relative to the electromagnet

A.2 NV-AFM

A.2.1 Coating AFM probes with poly-l-lysine

We use poly-l-lysine powders to make 0.01% w/v poly-l-lysine water solution. A 3-axis micromanipulator is used to control the position of the AFM probe: the AFM probe is stuck to the end of a think stick, which is held by the micromanipulator. Obtain a small drop of the poly-l-lysine solution on a glass slide. Move the AFM probe until its tip (and only the tip) immerses in the droplet. Lift the probe and wait several minutes for it to dry.

A.2.2 AFM procedures of attaching nanodiamonds

TESPA AFM cantilevers are used in this experiment. A general procedure of attaching nanodiamonds using the AFM contact mode:

1. Coat the AFM probe with poly-l-lysine
2. Locate an area on the sample with desired amount of nanodiamonds using the AFM built-in camera
3. Perform a large range scan using tapping mode with high setpoint (we used $\sim$22nm)
4. Find the desired scan area on the obtained scan and zoom in on the region, record X and Y offsets
5. To attach multiple nanodiamonds, retreat the probe, switch to contact mode, and scan the area using the X and Y offsets recorded
6. To attach single nanodiamond, follow the procedures below:
   (a) Locate the single nanodiamond on the scanning image obtained from tapping mode
   (b) Zoom in on the single nanodiamond

(c) Gradually lower the setpoint

(d) Keep trying until the single nanodiamond disappears from the scanning region

(e) Zoom out and perform the scanning again with higher setpoint. In most of the cases the nanodiamond is moved outside the scanning region instead of attached to the probe

(f) Keep trying until you made it

Acknowledgements

Finally finishing up my thesis dissertation, it is still hard to believe that my undergraduate study is coming to an end. I can still recall that one and half years ago, when I was trying to start my undergraduate research, I was going through countless websites of different research goups and never felt so lost. I was so excited when I heard back from Professor Hammel about the undergraduate research opportunity in this group, and here I am, 18 months later, still believe that this is the best thing happened to me in my 4.5 years at Ohio State.

First of all I would like to thank Professor P. Chris Hammel for giving me this opportunity to work with the most incredible group of people. You showed me how a successful scientist should be and inspired me to pursue a career in physics. I would not become who I am today without you. Thank you for all your guidances not only on my research projects, but also on how to be a successful researcher. Thank you for your trust and confidence in me. You encouraged me to keep perfecting myself and going further in academia.

I want to thank Vidya Bhallamudi. You have taught me so much, in physics, experimental techniques, communication skills, everything. You are always patient to me no matter how trivial my questions are or how many times I have asked. Thank you for trusting me to have my own research projects and letting me be creative with them (and thank you for working late with me when my creativity didn't work and caused problems). Thank you for pointing out new directions every time I was in a (seemingly) dead-end. Thank you for encouraging me thinking independently and trusting my judgments. Your helps and mentoring made me more than just an undergraduate student, but an independent researcher.

I also want to thank Brendan McCullian, my mentor/friend who just reminded me to write a good acknowledgment. I know you want to see me write my appreciation out loud so here you go–thank you for make the lab so much fun, for make all the hardcore physics understandable, and for help me with my GRE, PGRE, grad school applications, abstracts, posters, classes, thesis,

etc. Most importantly, thank you for encourage me every time when I feel down and tell me that everything will be OK.

Thanks to Carola Purser for guiding me through the first few months of my research. Getting started is the hardest part on everything, but somehow you made it easier. You helped me with my first project when I had absolutely no clue of my research; you helped me writing my first abstract and won the scholarship; you spent countless hours sitting in front the AFM with me trying to pick up a nanodiamond. Thanks for all the time you spent with me and the guidances you gave me.

Thanks to Dominic Labanowski for bringing my ADFMR project and spending many days during his break to discuss all the data with me.

Thanks to Bill Ruane and Shane White, who always stop by my posters and talk to me about my projects. Thanks to Camelia Selcu, Simran Singh, and Mike Page for helping me with AFM operations and imaging.

Lastly, thanks to my parents and friends for all their supports. I could not do this without you!

Bibliography

[1] A. Cuche, Y. Sonnefraud, O. Faklaris, D. Garrot, J.-P. Boudou, T. Sauvage, J.-F. Roch, F. Treussart, and S. Huant, "Diamond nanoparticles as photoluminescent nanoprobes for biology and near-field optics", *Journal of Luminescence*, vol. 129, no. 12, pp. 1475 –1477, 2009, Special Issue based on The 15th International Conference on Luminescence and Optical Spectroscopy of Condensed Matter (ICL'08), ISSN: 0022-2313. DOI: http://doi.org/10.1016/j.jlumin.2009.04.089. [Online]. Available: http://www.sciencedirect.com/science/article/pii/S0022231309002786.

[2] L. Rondin, J.-P. Tetienne, P. Spinicelli, C. D. Savio, K. Karrai, G. Dantelle, A. Thiaville, S. Rohart, J.-F. Roch, and V. Jacques, "Nanoscale magnetic field mapping with a single spin scanning probe magnetometer", *Applied Physics Letters*, vol. 100, no. 15, p. 153 118, 2012. DOI: 10.1063/1.3703128.

[3] S. Hong, M. S. Grinolds, L. M. Pham, D. Le Sage, L. Luan, R. L. Walsworth, and A. Yacoby, "Nanoscale magnetometry with nv centers in diamond", *MRS Bulletin*, vol. 38, no. 2, 155–161, 2013. DOI: 10.1557/mrs.2013.23.

[4] C. S. Wolfe, V. P. Bhallamudi, H. L. Wang, C. H. Du, S. Manuilov, R. M. Teeling-Smith, A. J. Berger, R. Adur, F. Y. Yang, and P. C. Hammel, "Off-resonant manipulation of spins in diamond via precessing magnetization of a proximal ferromagnet", *Phys. Rev. B*, vol. 89, p. 180 406, 18 2014. DOI: 10.1103/PhysRevB.89.180406. [Online]. Available: https://link.aps.org/doi/10.1103/PhysRevB.89.180406.

[5] M. R. Page, F. Guo, C. M. Purser, J. G. Schulze, T. M. Nakatani, C. S. Wolfe, J. R. Childress, P. C. Hammel, G. D. Fuchs, and V. P. Bhallamudi. (2016). Optically detected ferromagnetic resonance in metallic ferromagnets via nitrogen vacancy centers in diamond. arXiv: 1607.07485.

[6] D. Labanowski, A. Jung, and S. Salahuddin, "Power absorption in acoustically driven ferromagnetic resonance", *Applied Physics Letters*, vol. 108, no. 2, p. 022 905, 2016. DOI: 10.1063/1.4939914.

[7] L. Dreher, M. Weiler, M. Pernpeintner, H. Huebl, R. Gross, M. S. Brandt, and S. T. B. Goennenwein, "Surface acoustic wave driven ferromagnetic resonance in nickel thin films: Theory and experiment", *Physical Review B*, vol. 86, no. 13, 2012. DOI: 10.1103/physrevb.86.134415.

[8] C. Bradac, T. Gaebel, and J. R. Rabeau, "Nitrogen-vacancy color centers in diamond: Properties, synthesis, and applications", in *Optical Engineering of Diamond*. Wiley-VCH Verlag GmbH and Co. KGaA, 2013, pp. 143–175, ISBN: 9783527648603. DOI: 10.1002/9783527648603.ch5. [Online]. Available: http://dx.doi.org/10.1002/9783527648603.ch5.

[9] R. Schirhagl, K. Chang, M. Loretz, and C. L. Degen, "Nitrogen-vacancy centers in diamond: Nanoscale sensors for physics and biology", *Annual Review of Physical Chemistry*, vol. 65, no. 1, pp. 83–105, 2014, PMID: 24274702. DOI: 10.1146/annurev-physchem-040513-103659.

[10] C. P. Slichter, "Effect of alternating magnetic fields", in *Principles of magnetic resonance*. Springer-Verlag, 1989, 18–22.

[11] C. Kittel, "Ferromagentic resonance", in *Introduction to Solid State Physics*. Wiley, 1966, 379–382.

[12] G. Binnig, C. F. Quate, and C. Gerber, "Atomic force microscope", *Phys. Rev. Lett.*, vol. 56, pp. 930–933, 9 1986. DOI: 10.1103/PhysRevLett.56.930. [Online]. Available: https://link.aps.org/doi/10.1103/PhysRevLett.56.930.

[13] A. W. Schell, G. Kewes, T. Schröder, J. Wolters, T. Aichele, and O. Benson, "A scanning probe-based pick-and-place procedure for assembly of integrated quantum optical hybrid

devices", *Review of Scientific Instruments*, vol. 82, no. 7, p. 073 709, 2011. DOI: 10.1063/1.3615629.

[14] A. Cuche, A. Drezet, Y. Sonnefraud, O. Faklaris, F. Treussart, J.-F. Roch, and S. Huant, "Near-field optical microscopy with a nanodiamond-based single-photon tip", *Opt. Express*, vol. 17, no. 22, pp. 19 969–19 980, 2009. DOI: 10.1364/OE.17.019969. [Online]. Available: http://www.opticsexpress.org/abstract.cfm?URI=oe-17-22-19969.

[15] Y. Wang, Y. Zhang, B. Li, J. Lü, and J. Hu, "Capturing and depositing one nanoobject at a time: Single particle dip-pen nanolithography", *Applied Physics Letters*, vol. 90, no. 13, p. 133 102, 2007. DOI: 10.1063/1.2714287.